High-Sensitivity Inter-Satellite Optical Communications using Chip-Scale LED and Single Photon Detector Hardware

Research Article | Vol. 29, No. 7 / 29 March 2021 / Optics Express 10749
Optics EXPRESS

High-sensitivity inter-satellite optical communications using chip-scale LED and single-photon detector hardware

ALEXANDER D. GRIFFITHS,[1] JOHANNES HERRNSDORF,[1,*] ROBERT K. HENDERSON,[2] MICHAEL J. STRAIN,[1] AND MARTIN D. DAWSON[1]

[1] *Institute of Photonics, Department of Physics, University of Strathclyde, Glasgow, UK*
[2] *CMOS Sensors & Systems Group, University of Edinburgh, Edinburgh, UK*
[*] *johannes.herrnsdorf@strath.ac.uk*

Abstract: Small satellites have challenging size weight and power requirements for communications modules, which we address here by using chip-scale light-emitting diode (LED) transmitters and single-photon avalanche diode receivers. Data rates of 100 Mb/s have been demonstrated at a sensitivity of −55.2 dBm, and simulations with supporting experimental work indicate ranges in excess of 1 km are feasible with a directional gain of up to 52 dBi and comparatively modest pointing requirements. A 750 m, 20 Mb/s link using a single micro-LED has been demonstrated experimentally. The low electrical power requirements and compact, semiconductor nature of these devices offer high data rate, high sensitivity communications for small satellite platforms.

1. Introduction

In recent years, the development and deployment of small satellites has increased rapidly [1]. Many proposed applications require constellations, clusters or networks of such small satellites, necessitating the development of high speed inter-satellite data connections operating under strict size, weight and power (SWaP) budgets. While "small satellite", can define a range of satellite sizes and masses, the CubeSat standard has greatly increased academic and commercial access to space. These satellites are constructed in multiples of $(10\ \text{cm})^3$, 1 kg "1U" units, with such satellites commonly constructed with up to 6U. On-board communication systems for CubeSats are typically radio-frequency (RF) based. While RF communication is a mature technology, high data rate or high sensitivity links can require components with high power consumption and large size. Optical wireless communications are an attractive alternative due to the potential for high data rate systems with lower SWaP requirements [2]. Low SWaP light-emitting diode (LED) and single-photon avalanche diode (SPAD) systems for such applications are the focus of this paper.

Optical inter-satellite links (ISLs) for large satellites have been demonstrated for long ranges and at Gb/s data rates [3]. ISLs in low-earth orbit (LEO) and geostationary orbit (GEO) have been achieved using phase coherent lasers for high sensitivity, power-efficient communications. These systems outperform approaches based on intensity modulation, but are significantly more complex and costly [4]. While the mass and power requirements for such high performance, coherent links is low compared to RF technology, they are arguably beyond the restrictions of smaller satellites. For example, the Tesat laser communication terminals have a mass of 35 kg and a power consumption of 120 W [5,6]. Off-the-shelf free space communications systems for terrestrial applications with Gb/s data rates typically occupy a volume of 4U-6U, consume 20-45 W, and have very demanding pointing requirements. The pointing requirements can be relaxed by appropriate optics design at the cost of a lower data rate, however, the SWaP footprint remains

#421101 https://doi.org/10.1364/OE.421101
Journal © 2021 Received 29 Jan 2021; revised 10 Mar 2021; accepted 11 Mar 2021; published 22 Mar 2021

Optics EXPRESS

challenging for small satellites. Most current programs for CubeSat ISLs therefore focus on RF technology [7].

Most of the research into optical communications for CubeSats was focused on intensity modulation for satellite to ground links, such as NASA's optical communications and sensors demonstration program [8] and the nanosatellite optical downlink experiment from MIT [9]. Similar systems have been proposed for ISLs [10] or a LEO communication relay system [11]. These experiments typically use laser diodes (LDs) with fiber amplifiers as transmitters. The SWaP requirements for these systems are well within the capability of CubeSats, though they typically occupy at least a full 1U module and require significant battery power for operation. Additionally, the narrow beams from laser systems often have sub-mrad divergences, therefore requiring tight optical alignment of satellites, which can be difficult in the CubeSat form-factor.

Intensity modulated optical communication has been shown to provide multi-Gb/s data rates over free space [12], and is expected to be part of the next generation of wireless communication systems [13]. Additionally, high sensitivity receivers and optimized transmission schemes enable data transmission with very low levels of received power [14–16]. Typically, high data rate and high sensitivity experiments are performed using large, complex or high power consumption equipment, such as arbitrary waveform generators, lasers with external modulators and superconducting cryogenic receivers. Further encoding and decoding complexity is introduced when high order modulation and multiplexing techniques are employed [12]. These transmitter and receiver hardware requirements can be problematic under strict SWaP constraints.

LEDs are a potential alternative device suitable for ISLs [17,18], bringing further advantages in SWaP constraints over laser systems, along with reduced complexity, longer lifetimes and lower cost. Gallium nitride (GaN) micro-LEDs with dimensions less than 100 μm offer high modulation bandwidths and data rates comparable to the CubeSat laser systems [12]. Micro-LEDs can be fabricated in high-density array format and bump-bonded to complementary metal-oxide-semiconductor (CMOS) control electronics, providing compact, integrated devices with a digital interface [19]. The high degree of spatial and temporal control over the optical emission of these devices, makes them attractive as transmitters for optical communications [20,21]. While the angular divergent nature of LED emission may reduce potential ISL ranges, it relaxes the tight pointing requirements found in laser systems.

Recently, SPADs, *i.e.* avalanche photodiodes driven in Geiger mode, have attracted interest for high sensitivity optical communications [22]. By fabricating arrays of SPADs and combining the outputs in either a digital or analog fashion, the dynamic range can be increased while maintaining single-photon sensitivity with the highest photon detection probability typically in the blue-green and sometimes red wavelength region [23–25]. As SPAD fabrication is compatible with CMOS technology, highly integrated receiver systems can be developed, with signal processing performed on-chip [26,27]. The single-photon nature of these receivers allows exceptionally high sensitivity levels to be reached, moving closer to the standard quantum limit (SQL) than more conventional avalanche photodiodes (APDs) [27]. The SQL is determined by the Poissonian nature of photon detection, and gives the minimum number of photons required to achieve a given BER [28,29]. When considering specific data rates and photon wavelengths, this gives a limit on receiver sensitivity, usually quoted in dBm. At 100 Mb/s, with 635 nm light, sensitivities as low as −51.6 dBm have been demonstrated, 18.5 dB from the SQL of −70.1 dBm [28].

Here, we present an optical communication link implemented with a CMOS controlled micro-LED transmitter and a SPAD array receiver, both realized with low SWaP integrated electronic systems. Our work underpins the prospect for using chip-scale transmitter and receiver elements for ISLs, enabling transceiver systems occupying a fraction of 1U. While having smaller dimensions than laser-based systems, our proposed system still achieves up to 52 dBi directional gain and thus a significant benefit over similarly small RF systems. First, ray-tracing simulations

Optics EXPRESS

are presented, to determine the potential range, coverage and data rate characteristics of the link based on simple optics and the known receiver sensitivity. To verify that the simulated performance can be realized, a demonstrator system was constructed and tested. Using a simple transmission scheme, data rates of 50 and 100 Mb/s are demonstrated in the laboratory with sensitivities of −60.5 and −55.2 dBm, respectively, which is 13.4 dB from the SQL. At an example terrestrial demonstration distance of 750 m, a 20 Mb/s communication link was established, validating the simulations. The combined power consumption of the current, unoptimized system is less than 5.5 W, demonstrating that these devices can provide high performance optical communication links on strict SWaP budgets. The simulations, supported by experimental work, suggest such simple optical systems can be used to provide high data rate signals over kilometer ranges, with relaxed pointing requirements.

2. Range and coverage simulation

To justify the potential use of micro-LED and SPAD based communication links for ISLs, a performance envelope was determined using ray tracing simulations [30], performed using Zemax OpticStudio. The LED was modeled as an area emitter, and the effect of its spatial extend on the beam divergence was found to dominate over any possible diffraction limitations, which were therefore ignored. To determine the communication capabilities, the optical power incident on the receiver must be calculated. Therefore, the simulations were set up to determine intensity maps at varying distances away from the transmitter, up to 10^6 m. With knowledge of the receiver sensitivity, and by defining a collection aperture size, a maximum achievable data rate can be determined for a given range and angle of coverage. The parameters used for simulation are summarized in Table 1, reflecting typical micro-LED transmitter properties, and assuming a receiver aperture up to 10 cm diameter, which is likely to be the largest achievable with a CubeSat system.

Table 1. General simulation parameters and assumptions.

Parameter	Value
Emitted power	1 mW
Ray tracing software	Zemax OpticStudio
# of rays traced	1×10^8
Emission wavelength	450 nm
Emission linewidth	20 nm
LED emission profile	Lambertian, Eq. (1)
LED emitter area	100×100 μm^2
Tx Optics	Aspheric lenses up to 1" diameter
Transmission distance	Up to 1×10^6 m
Rx aperture	Up to 10 cm diameter
Encoding scheme	RZ-OOK
Data rate	1 kb/s – 100 Mb/s
Target BER	2×10^{-3}
Target Rx power	Based on fit in Fig. 2
Transmitter angle	Indicated in Figs. 4, 5, and 6
Receiver angle	Directed at transmitter

Three transmitter optical systems were considered: (i) no lens, (ii) collimation with a Thorlabs C240 lens, and (iii) collimation with a Thorlabs ACL25416 lens. Both lenses were used in

Optics EXPRESS

the experimental implementations detailed later, and are inexpensive, simple, and permit good collimation of LED light. The C240 lens was chosen for its high numerical aperture (NA) and small size. The ACL25416 has a higher NA than the C240, therefore collecting more of the divergent micro-LED emission. However, this comes at the expense of increased system size due to a longer focal length, larger lens diameter and increased thickness. The parameters for both lenses are summarized in Table 2. It is also interesting to consider the case where the transmitter has no collimation optics and operates with the full Lambertian profile, *i.e.* the the angular intensity profile $I(\theta)$ varies with emission angle θ according to Eq. (1).

$$I(\theta) \propto \cos\theta. \tag{1}$$

Table 2. Effective focal length (*EFL*), numerical aperture (*NA*), diameter (*D*) and thickness (*S*) of the aspheric lenses.

Lens	*EFL* (mm)	NA	D (mm)	S (mm)
C240	8	0.50	9.9	3.4
ACL25416	16	0.79	25.4	14.1

The simulated received intensity values for a point-to-point, aligned link are shown in Fig. 1. The intensity falls off following the inverse quadratic trend expected for the diverging beam, with the higher NA lens significantly increasing the intensity at longer ranges. To determine achievable data rates with these intensity values, the receiver area and sensitivity must be known.

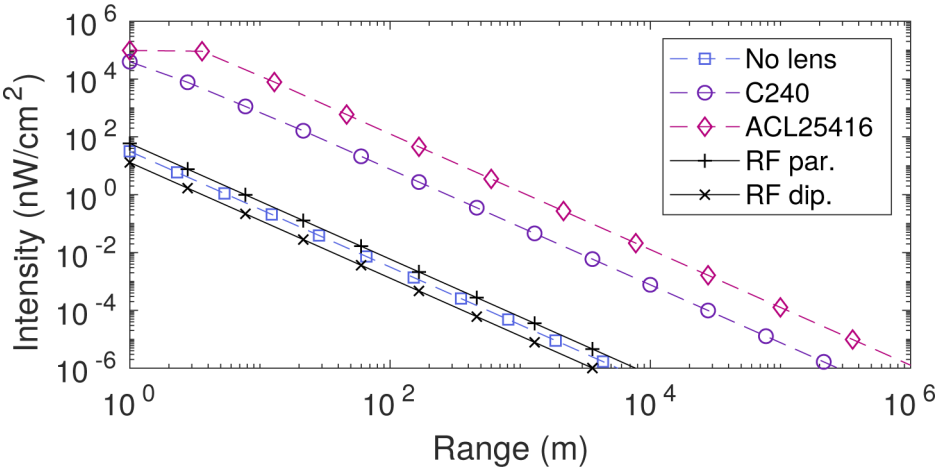

Fig. 1. Simulated received intensity at increasing range, following the expected inverse quadratic trend. Also shown are the received intensities for a 10 cm diameter parabolic RF antenna and a half-wave dipole RF antenna.

A clear benefit of optical systems over RF systems under strict SWaP restrictions can be seen in Fig. 1. The C240 and ACL25416 lenses result in significant increases in the received intensity due to the high directionality achieved with them. Even the larger of these two lenses is just one inch in diameter, which is similar to the wavelength of typical RF signals. RF systems with the same dimensions would therefore have little directionality. Figure 1 includes the analytically calculated received intensity of a half-wave dipole antenna (2.15 dBi directional gain), assuming that the emitter power is also 1 mW as assumed for the LED in the simulations. It can be seen that the received intensity of the dipole antenna transmitter is even less than for the bare LED. If

Optics EXPRESS

extending to the maximum considered dimensions of 10 cm, then a parabolic RF antenna can be used to achieve a limited degree of directionality. The angular emission pattern of a parabolic antenna is given by Eq. (2):

$$I(\theta) \propto \left| \frac{2c}{\pi D f} \frac{J_1((\pi D f/c) sin(\theta))}{\sin(\theta)} \right|^2 . \tag{2}$$

Where θ is the emission angle, $I(\theta)$ is the angular intensity profile, D is the antenna diameter, f the carrier frequency, c the speed of light, and J_1 a first order Bessel function.

Figure 1 contains the received intensity for $D = 10$ cm, and $f = 14.5$ GHz, obtained by integrating Eq. (2) over the solid angle covered by the receiver, which is still significantly lower than with the optical systems with lenses. The received intensity data from Fig. 1 can be translated into directional gain, which is listed in Table 3, and is the intensity gain due to the directionality of the transmitter compared to an isotropic transmitter. The bare LED, despite being microscopic in size, has already a higher gain than a half-wave dipole. However, the systems with lenses have between 30 dB and 50 dB higher gain than the RF systems, *i.e.* an RF system would require a receiver with up to 50 dB better sensitivity than the single photon detector employed here to match the performance of our system. Note that this benefit over RF is a direct consequence of the small dimensions of the transmitter making it physically challenging to achieve any directionality of the RF signal.

Table 3. Directional gain of the different LED-based transmitters considered here compared to cube-sat compatible RF systems.

System	directional gain (dBi)
bare LED	5.99
LED + C240 lens	39.8
LED + ACL25416 lens	52.0
RF half-wave dipole antenna	2.15
RF 10 cm parabolic antenna	8.73

Due to the lower shot noise in RF frequencies, RF receivers can have high sensitivities. For example, receivers for the IEEE 802.11a/b/c standards often have sensitivities near −75 dBm at 50 Mb/s. Therefore, the net benefit of the optical system over comparable RF systems is 16–35 dB. As the received power in the far field drops inverse quadratically with distance, this translates into a 6×–56× longer transmission distance of the optical system at the same transmitter power.

As discussed above, receiver sensitivity gives the minimum required incident power to achieve a given BER at a specified data rate and wavelength. Typically, a BER target between 2×10^{-3} and 1×10^{-2} is used to enable forward error correction codes to achieve an output BER of 1×10^{-9} [31] or better. The red cross markers in Fig. 2 show the sensitivity for a custom SPAD array receiver [25], detailed further in Section 3.1. The SQL for return-to-zero (RZ) on-off-keying (OOK) a BER of 2×10^{-3} and wavelength of 450 nm can be calculated by Eq. (3) and is indicated in the Fig. 2, demonstrating the high sensitivity nature of this receiver.

$$\mathrm{SQL} = -\frac{hcR}{2\lambda} \log(\mathrm{BER}). \tag{3}$$

Where R is the bitrate, λ is the emission wavelength, h is the Planck constant and c is the speed of light.

It is noted that the experimental results show a constant separation in dB from the SQL, which is to be expected as the number of photons detected per bit should remain the same for a given

Optics EXPRESS

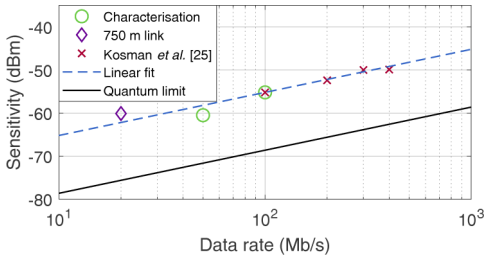

Fig. 2. Sensitivity limit at a BER of 2×10^{-3} for given data rates using RZ-OOK encoding. Our experimental characterisation work is shown along with work from Kosman *et al.* using the same receiver [25]. In addition, the result from a 750 m link detailed in Section 3.4 is shown which had a lower BER of 1×10^{-5}.

BER. The linear fit shown in Fig. 2 maintains the average separation of the experimental data from the SQL, and can be used to relate a received power level to an achievable data rate. The results using the same receiver and micro-LEDs in this work, detailed in Section 3.2, are also shown in green circles. These results lie reasonably close to the linear fit. Additionally, the result from a 20 Mb/s long distance demonstration detailed in Section 3.4 is shown, though it should be noted that due to experimental constraints the BER was lower than 2×10^{-3}.

By combining the linear fit in Fig. 2 and the intensity data in Fig. 1, the relationships between range, angular displacement, data rate and optical set-up can be determined. The resulting data rates for the point-to-point, aligned link are shown in Fig. 3. Note that the data rate has been upper-end clipped at 100 Mb/s as this is the limit of the transmitter firmware used in Section 3.1.

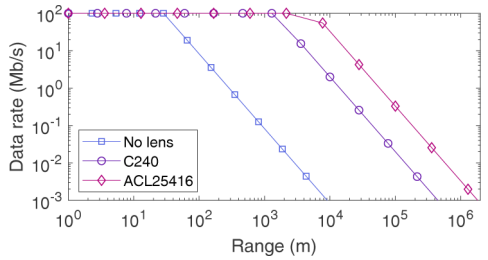

Fig. 3. Simulated achievable data rates for a given range, based on the intensity data of Fig. 1 and the approximation in Fig. 2.

A summary of achievable ranges for a selection of data rates is shown in Table 4. The results suggest that useful data rates are possible over ranges up to 100s of kilometers. It is difficult to suggest target ranges and data rates as system requirements will vary strongly with different satellite application scenarios. Formation-flying satellites may be separated by less than 10 km [17], while 1000 km is a typical LEO-ground distance [11]. The fact that the performance envelope for this communication link sits within these ranges is promising.

Table 4. Achievable point-to-point ranges for 100 Mb/s, 1 Mb/s, and 10 kb/s.

Setup	100 Mb/s	1 Mb/s	10 kb/s
No lens	28.5 m	287 m	2.87 km
C240	1.41 km	14.1 km	141 km
ACL25416	5.74 km	57.4 km	574 km

Optics EXPRESS

The lens-collimated light from the LED is still divergent, causing losses and limiting the range for a point-to-point link. Importantly though, this divergent light can be thought of as providing a level of coverage over an angular region, reducing the pointing accuracy reqirement. With the simulated intensity maps, the achievable range for a given data rate at a given angle from the transmitter axis can be determined. The results are shown in Fig. 4 as angular plots. Note that the radial axis is logarithmic, and in the case of Figs. 4(b) and 4(c), the angular axis has been expanded in order to observe the profiles.

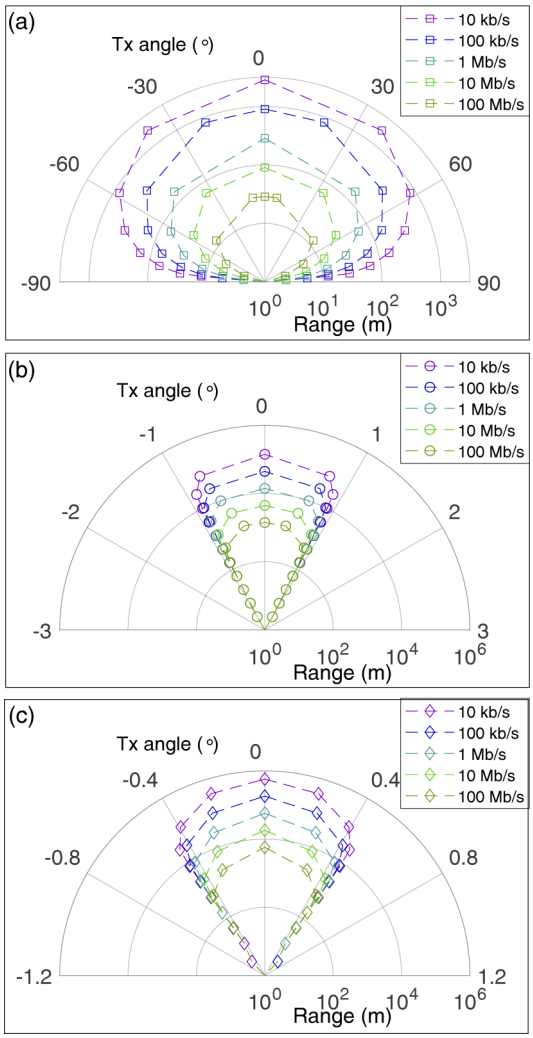

Fig. 4. Simulated angular coverage and range performance at data rates from 10 kb/s to 100 Mb/s for (a) no lens, (b) C240 and (c) ACL25416. Note the angular ranges in (b) and (c) have been adjusted to aid visualisation of the narrow beam cases.

In Fig. 4(a), with no lens, the micro-LED provides almost 60° angular coverage due to the Lambertian emission profile. For example, a 100 Mb/s link can be maintained over 60° at a 10 m range, and at 10 kb/s, the same angular coverage is maintained at approximately 1 km. The collimated light in Figs. 4(b) and (c), while still divergent, produce much tighter beams. As the light is more directional, the range is greatly increased at the expense of angular coverage. The

Optics EXPRESS

C240 and ACL25416 lenses provide angular coverages of roughly 1 and 0.4 degrees (17.45 and 6.98 mrad), respectively.

As discussed in the introduction, alternative systems for CubeSat optical communications often use LDs. For this reason, the performance of the same optics with a LD source were simulated for comparison. Parameters were chosen to simulate a Thorlabs PL450B LD, which emits at 450 nm, and was assumed to have a parallel beam divergence of 7.5 degrees, and a perpendicular beam divergence of 21.5 degrees, based on the manufacturer's data. The emitted power was set to 1 mW for comparison to the micro-LED. The resulting beam coverages along the narrow divergence axis for a 100 Mb/s link are shown in Fig. 5, with the micro-LED data also shown. For the no lens and C240 cases, the micro-LED provides significantly wider coverage, at the expense of range. However, for the ACL25416, the coverage and ranges are similar for all but the point-to-point case. This is attributed to the lens collecting and collimating more of the micro-LED light than the C240 due to a higher NA, but for the LD, the increase in NA is irrelevant due to the small NA of the LD, and the longer focal length of the lens results in a wider beam diameter.

In addition to the range and angular coverage comparison with LDs, it is important to consider the practicalities of implementing LD or micro-LED transmitter. While both are mm-scale optical devices, the micro-LED chip is integrated with CMOS control electronics, allowing modulation, control and power to be supplied by digital signals applied directly to the device. A LD system would require an appropriate current driver and cooling systems to operate and maintain a good lifetime, taking additional space in the satellite. The LD can of course produce far higher power than the 1 mW simulated here, which would further increase the range. Additionally, many of the systems described in the introduction implement fiber amplifiers to further increase the output optical power. In addition to the increased electrical power consumption from such hardware, this also results in systems which can take up a full 1U part of a CubeSat, whereas the micro-LED system could be a single 10×10 cm^2 printed circuit board (PCB), or possibly even mounted on the satellite chassis. The choice of transmitter technology will be application specific, with micro-LEDs able to provide a simple, low cost, low SWaP, robust system, with shorter range, but relaxed pointing requirements.

In the previous simulation results the receiver aperture has been assumed to have a diameter of 10 cm. Collecting light from an area this size on to the few mm^2 sized SPAD receiver would require bulky or complex optics, so it is important to consider the effect of smaller apertures. Figure 6 shows the variation in angular coverage for a 1, 5 and 10 cm aperture, respectively, using the ACL25416 lens and considering a data rate of 100 Mb/s. The achievable range increases in a linear fashion with increasing aperture size, because the drop in intensity as a function of range and the detector area as a function if aperture size both follow quadratic laws.

It is not yet clear what ISL distances will be realistic in CubeSat applications. However, the ray tracing simulations suggest that a micro-LED and SPAD based optical communication link can achieve useful data rates and coverage levels for ISLs up to 10s of km. The interplay between optical set-up, range, coverage and data rate seen in these results suggest that the system can be optimized based on a target application.

Optics EXPRESS

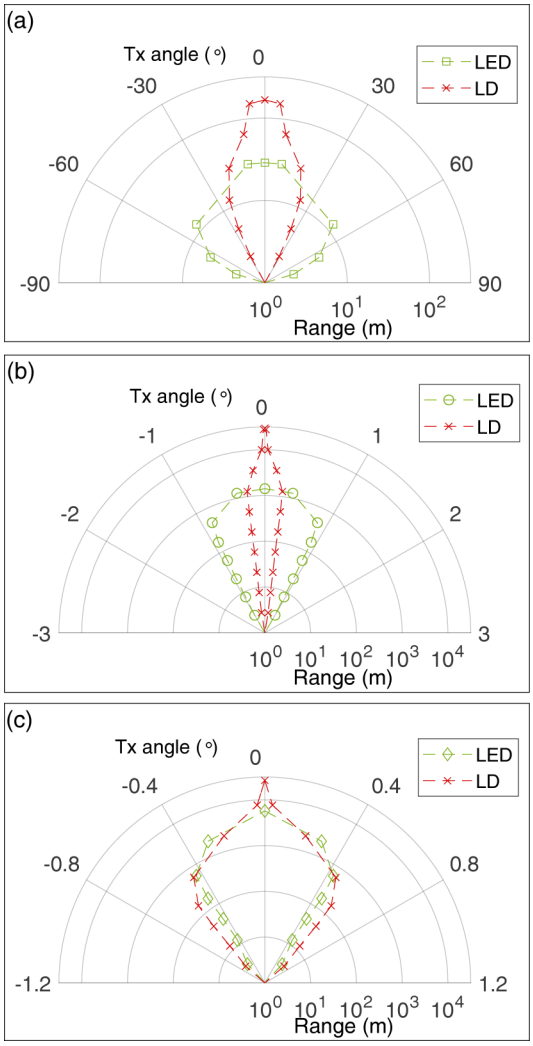

Fig. 5. Simulated LED-based transmitter performance compared to LD system with the same emitted power of 1 mW and target data rate of 100 Mb/s for (a) no lens, (b) C240, (c) ACL25416. The LD consistently provides longer point-to-point ranges with much tighter pointing requirements for low numerical aperture cases.

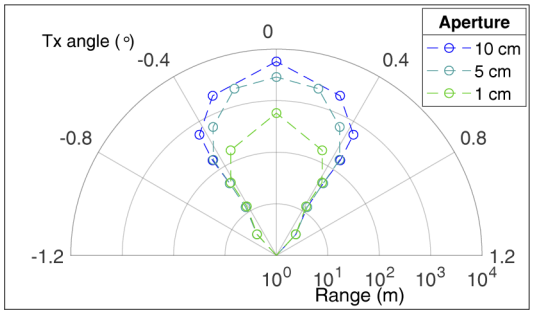

Fig. 6. Simulation of angular coverage for a 100 Mb/s link using the ACL25416 lens with varying aperture size.

Optics EXPRESS

3. Experimental verification

With a performance envelope having been defined by ray-tracing simulation, a demonstrator system was constructed to verify that such a system is attainable within the strict SWaP constraints of CubeSats. We note that both GaN LEDs and Si SPADs have been used in separate space missions before [32–34], and other components are standard silicon electronics. There may be some degradation in SPAD performance, in particular an increase in the dark count rate, due to LEO radiation during the course of a mission. Based on the experiences of these earlier missions, the degradation during a typical LEO CubeSat mission should remain within limits that are acceptable for this application. Furthermore, it may be possible to partially recover radiation damage by annealing [35,36].

3.1. Transmission scheme and hardware description

The data transmission scheme employed here is RZ-OOK. The implementation of this scheme is simple, as the transmitter modulates between two output intensity levels, and the receiver can decode the data stream with a single threshold. Having only two intensity levels also means that data reception will not be adversely affected by saturation of the SPAD by the received signal. Despite the higher bandwidth requirements, RZ transmission was chosen over non-RZ (NRZ) as it has been show to improve bit error ratio (BER) performance in SPAD based systems by reducing inter-symbol interference (ISI) [28,37]. In NRZ-OOK, the timing jitter of photon detection events and after-pulsing can cause an overflow into the next bit period. However, in RZ-OOK, there is an interval within each bit period in which no photons are sent, reducing the probability that detection events overflow.

The experimental arrangement is shown schematically in Fig. 7, and was operated in a dark laboratory [38]. The transmitter used a single, 99×99 μm^2 pixel from a 16×16 array of micro-LEDs. The fabrication details and characterization of similar devices are reported in Refs. [20,39]. The micro-LED array is flip-chip bonded to CMOS control electronics, enabling active-matrix control. The device is housed on an evaluation PCB where a field-programmable gate array (FPGA) (Opal Kelly XEM3010) provides control signals. The emission wavelength was 450 nm, though we note that such devices can be fabricated with wavelengths from the UV-C band to green with nitride alloys, which also covers the high sensitivity response region of Si SPADs. Thus, the wavelength can be chosen, for example, to match many of the solar Fraunhofer lines, which may offer a low background noise channel [18].

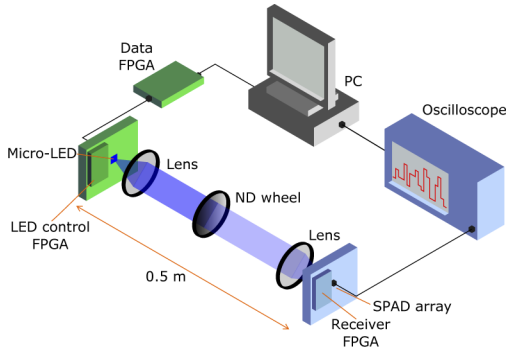

Fig. 7. Schematic of the laboratory-based experimental setup.

An additional FPGA module (XEM6310) was used as a data source, providing a pseudorandom bit sequence (PRBS) preceded by a pilot signal to mark the start of the sequence. By outputing the PRBS with a 50% duty cycle, the selected pixel of the LED array produces the desired

Optics EXPRESS

RZ-OOK output. The LED is modulated full on-off by the CMOS driver and has a bandwidth of 110 MHz when driven in this fashion [39], which leads to a reduction of transmitter power at data rates of 100 Mb/s or more, because at this rate the RZ-OOK scheme encodes ones as pulses with only 5 ns duration. The data rate can be adjusted by changing the output frequency of the FPGA. In the following experiments, data rates of 50 and 100 Mb/s are used, limited by the FPGA firmware, resulting in RZ-OOK emitted average optical power of 390 μW and 188 μW, respectively.

For characterisation of the data transmission performance, the optical signal was collimated with a lens (Thorlabs C240TME-A) and transmitted over a distance of 0.5 m. A graded neutral density (ND) filter wheel (Thorlabs NDC-50C-4M-A) was used to control the attenuation of the signal reaching the receiver. A collection lens (Thorlabs ACL4532U) focused the light onto the active area of the optical receiver.

The receiver consists of 64×64 SPADs on a 21 μm pitch, with a fill factor of $F_{fill} = 43\%$ and operating at room temperature [25]. Including the surrounding electronics, the chip is 2.6×2.8 mm^2, and is packaged to interface with a PCB. A further FPGA (Opal Kelly XEM6310) provides control signals and power to the chip, and an external 15 V bias is applied to the SPAD pixels. The individual pixels have a photon detection probability (PDP) of $\eta_{PDP} = 26\%$ at 450 nm [40], a measured dark count rate of 350 events per second, and a dead time of 20 ns, *i.e.* the entire array has a higher dark count rate and a shorter effective dead time. The output of the SPADs, which operate in free-running mode, is combined using XOR trees and ripple counters so the device is operated as a digital silicon photomultiplier, with a single output of photon counts at a given sample rate [26,41]. For the experiments here, a 32×32 subset of the array was set as active, as a trade-off between total dark count level and dynamic range. Additionally, a pair of spectral filters (Thorlabs FEL0400 and FES0500, 450 nm center wavelength, 100 nm linewidth, 1.5 dB loss) were placed in front of the active area to reduce background counts.

The photon count signal from the chip is read out from low voltage differential signaling (LVDS) pads using a differential probe and oscilloscope. Using the FPGA interface, the array was set to output photon counts at a sampling rate of 200 MHz, with a range of 0-31 photon counts. The analog voltage signal from the LVDS pads was captured by the oscilloscope, resampled and digitized to recover a photon count signal. To decode the bit stream, photon counts are integrated over the bit period and compared to a threshold value.

As the output from the receiver is a number of photons at a given sample rate, the detected photons per second (Φ_{det}) is readily obtained from the oscilloscope trace. Incident photons per second (Φ_{inc}) can then be calculated according to:

$$\Phi_{inc} = \frac{\Phi_{det}}{\eta_{PDE}(1 - \Phi_{det}\frac{\tau_d}{N})}. \tag{4}$$

Here, N is the number of active SPADs, τ_d is the dead time of a single SPAD, and η_{PDE} is the photon detection efficiency of the array, given by $\eta_{PDE} = \eta_{PDP}F_{fill}$. Incident optical power P_{inc} is then given by:

$$P_{inc} = \Phi_{inc}E_{ph}. \tag{5}$$

where E_{ph} is the energy of a 450 nm photon.

3.2. Communication link characterization

To asses the BER performance of the communication link, a PRBS of 2^{15} bits was repeatedly transmitted until over 10^6 bits were received. Experiments were performed at various incident power levels, producing the BER curves in Fig. 8. The target BER threshold of 2×10^{-3} is plotted for reference. The slopes of the curves for 50 Mb/s and 100 Mb/s reflect the different power levels needed to get sufficient photons per bit. The 100 Mb/s curve approaches a BER floor near

Optics EXPRESS

a BER of 10^{-4} which is due to saturation effects of the SPAD array. The signal properties at the FEC threshold are summarized in Table 5. An incident optical power of 0.9 and 3.0 nW is required for 50 and 100 Mb/s, respectively, corresponding to sensitivities of −60.5 and −55.2 dBm. The results from Table 5 are also shown in Fig. 2 along with earlier LD work [25]. The fact that these results lie close to the linear fit used in the simulation indicates that using micro-LED transmitters does not compromise the high sensitivity nature of the link.

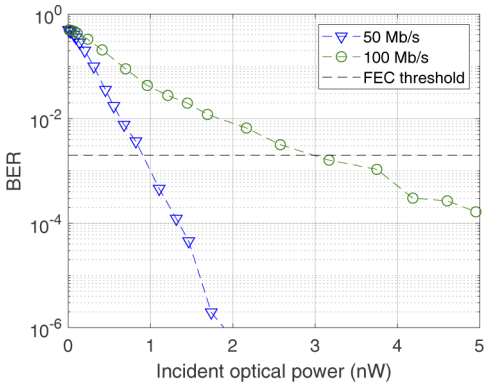

Fig. 8. BER against incident optical power incident on the receiver for data rates of 50 and 100 Mb/s over a link distance of 0.5 m.

Table 5. Received optical power (*P*) at the FEC threshold for 50 and 100 Mb/s, with corresponding sensitivity (*S*), power above the SQL (*D*), average detected photons per bit (ϕ_{det}) and average incident photons per bit (ϕ_{inc}).

R_{data} (Mb/s)	P (nW)	S (dBm)	D (dB)	ϕ_{det} (ph/bit)	ϕ_{inc} (ph/bit)
50	0.9	−60.5	11.1	4.6	41
100	3.0	−55.2	13.42	7.5	68

At 50 Mb/s with 450 nm photons and a target BER of 2×10^{-3}, the attained sensitivity of the system is 11.1 dB away from the SQL of −71.6 dBm. The 26% PDP and 43% fill factor accounts for 9.5 dB of the difference, with the remainder attributed to the effects of background and dark counts. This can be seen in Fig. 9(a), which shows the experimental probability distributions of photon counts for transmission of a binary "0" and "1" at the FEC threshold for 50 Mb/s. Both closely follow a Poisson distribution around their mean, and can be readily distinguished by applying a decision threshold. The non-zero count levels for transmission of a "0" push the threshold requirements to higher levels, increasing the power requirements above the SQL. Nevertheless, an average of only 4.6 detected photons is required to achieve the FEC threshold. Accounting for PDP and fill factor with Eq. (4), this corresponds to 41 incident photons per bit.

For 100 Mb/s, the attained sensitivity is 13.4 dB from the SQL of −68.6 dBm. It would be expected to remain the same separation as for 50 Mb/s, as the photon counts per bit should remain the same, however the separation is increased due to ISI. Figure 9(b) shows the probability distribution of counts for 100 Mb/s. Here it can be seen that the "0" level distribution is no longer Poissonian. In fact, it is the average of two Poisson distributions, associated with whether the previous transmitted bit was "0" or "1". If the previous bit is "1", some photons from the LED pulse trail into the next bit, due to a long pulse fall time. This pushes the decision threshold to a higher level, increasing the requirement on incident power for distinguishing a "1" from a "0". This limitation is dute to the 110 MHz bandwidth of the micro-LED [39],

Optics EXPRESS

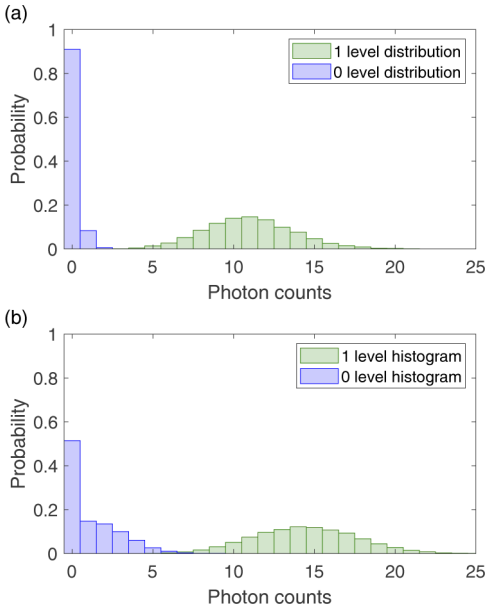

Fig. 9. Probability distributions of 0 and 1 level photon counts per bit for (a) 50 and (b) 100 Mb/s at a BER of 1×10^{-3}.

resulting in non-negligible rise and fall times in the optical response to a 5 ns electrical input. Despite this limitation, only 7.5 detected photons are required per bit to reach the FEC threshold, corresponding to 68 incident photons per bit.

Reference [27] provides a useful review of state-of-the-art high sensitivity SPAD receivers. The work presents an integrated SPAD receiver system with sensitivities of −51.2 and −46.3 dBm for 50 and 100 Mb/s with a BER of 2×10^{-3}. Sensitivities of −46.2 and −43.8 dBm for 150 and 200 Mb/s respectively are shown for a higher BER of 6.5×10^{-3}. In both cases a 635 nm laser with external modulator was used as the optical transmitter. Our work shows a sensitivity improvement of 14.3 and 11.4 dB, respectively, over the lower data rates at a wavelength of 450 nm, where the SQL is also higher due to the higher photon energy. While we are currently unable to reach data rates above 100 Mb/s due to limited FPGA output rates and micro-LED pulse widths, related work with the same receiver and a laser diode transmitter shows the same trend in sensitivity enhancement [25].

3.3. *Size, weight and power consumption*

Both transmitter and receiver used here are mm-size, chip-scale devices housing LEDs, drive electronics, photodetector arrays and receiver electronics. The current system houses these chips in ceramic packages connected to evaluation PCBs, which have dimensions and masses of 13×18.5 cm^2/241 g, and 12.5×20.5 cm^2/235 g, for transmitter and receiver, respectively. While this hardware is already at a PCB level and relatively compact and light, many parts of the evaluation boards would be unused in a final application, allowing transceiver systems to be developed on the scale of a few square centimeters. The masses of the LED and SPAD chips in ceramic packages are 7 g and 15 g respectively, and contain the majority of the functional elements of each system. The size and weight footprint of a size-optimized system will therefore be dominated by the receiver and transmitter optics, and a transceiver with similar optics as those used in this work should fit into a volume of ~0.2U.

Optics EXPRESS

The electrical power for the system is drawn by four elements: the data-, LED control-, and receiver- FPGA, and the receiver bias. Power for the micro-LED emitter and CMOS driver is drawn through the LED control FPGA. The SPAD photodetectors are powered through the receiver bias, while the surrounding electronics draw power through the receiver FPGA. The power consumption of the system is summarized in Table 6, with the transmitter and receiver combined consuming 5.48 W. The FPGA configurations used here include USB3 connections and firmware components for most functions except for clock synchronization and threshold determination, and therefore the power drawn by the FPGAs is representative of a fully embedded system. The current arrangement has not been optimized for power consumption, so this is an upper ceiling on the requirements. Power requirements can be readily reduced by streamlining the FPGA configurations into one single FPGA or application-specific integrated circuit. With an emitted optical power of 188 μW and 1-2% wall plug efficiency [20], we deduce that the power consumption of the transmitter is not dominated by the optical emitter. The SPAD receiver consumes 115 mW when considered without the FPGA [25]. Furthermore, many application areas already employ FPGAs or on-board computer systems which could be used to produce and process the digital signals, meaning only the LED and receiver hardware consume additional power and capacity in the CubeSat.

Table 6. Power consumption of components in the system, totalling 5.48 W.

Component	Power draw (W)
Data FPGA	0.95
LED control FPGA	1.00
Receiver FPGA	3.45
Receiver bias	0.08

In summary, an optimized LED and SPAD transceiver system requires less than 5.48 W and can be mounted on a single PCB weighing a few hundred grams. This is a significantly lower requirement than that of laser based ISLs.

3.4. Long range experimental verification

The characterization detailed in Section 3.2 was performed under idealized laboratory conditions, with low background light and a transmission distance of 0.5 m. In addition, the simulated data in Section 2. is an idealized case. To justify the use of micro-LEDs for space communications it is important to verify experimentally that significant ranges can be achieved under realistic conditions with the current hardware.

For an initial test, the setup from Section 3.2 was taken to a larger indoor space with roughly 40 m of clear line of sight. The transmitter and receiver were separated and the BER measured for different ranges. Distances greater than 40 m were achieved using a large mirror (COMAR 250 MC 160) to reflect the transmitted light. BER performance at 100 Mb/s is shown in Fig. 10. For all ranges, the BER reaches a floor below the FEC threshold of 2×10^{-3}. This floor is comparable to that observed in Fig. 8, and occurs as saturation effects begin to increase BER as incident power increases.

The inset in Fig. 10 shows the BER performance for the same experiment with the transmitter lens removed. As the emitted light is then much more divergent, the power loss is very rapid with increasing range. Nevertheless, the high sensitivity of the receiver enables a BER of less than 2×10^{-3} at a range of almost 2 m. This demonstrates that meter scale communication is possible with the full wide-angle emission of the micro-LED. The achieved range of less than 2 m is much shorter than the 29 m calculated in the simulations in Fig. 4(a). This is due to three major factors: the 45 mm diameter of the receiver collection lens is much smaller than the 10

Optics EXPRESS

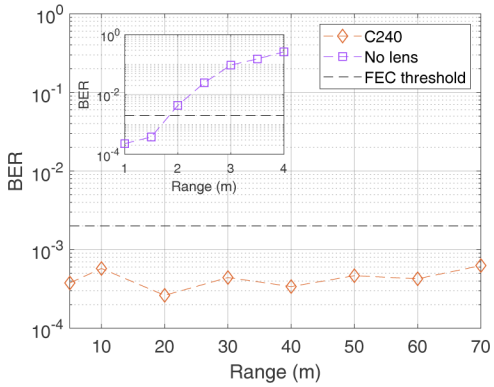

Fig. 10. BER performance for longer distance (up to 10's of meters) indoor measurements using the same experimental setup as in Section 3.2, with 188 μW emitted power at 100 Mb/s. Inset: BER performance for the same setup without the transmitter collimation lens.

cm diameter area assumed, the LED pixel emitted power of 188 μW is lower than the 1 mW assumption, and background counts will raise the requirements on incident power. Nevertheless, the results fall within the envelope of the simulations, and furher increasing transmitter power and receiver aperture is certainly feasible.

To further justify the practicality of the LED and SPAD based communication link, the system was tested over a longer ground based distance across the city of Glasgow, Scotland. A 750 m link distance was achieved with the transmitter mounted in the viewing platform of The Lighthouse (a tall public building), and the receiver in the University of Strathclyde's Livingstone Tower. A map of Glasgow city indicating the link is shown in Fig. 11(a). Experiments were performed after sunset to reduce background light. A video documentation of the experiment (Visualization 1) can be found in Ref. [42] and also at https://www.youtube.com/watch?v=5aorYup1BMg.

The optical setup was adjusted to improve performance. Due to the time window available for this experiment, only one transmitter configuration could be tested and the ACL25416 lens was used. On the receiver side, the collection lens was replaced with a set of camera optics with a focal length of 100 mm (Navitar MVL100M23), to reduce the field of view and thus the number of city lights within it. A 3D printed enclosure was used to block stray light from around the receiver, and a bandpass filter (Semrock FF01-440/40-25, 440 nm center wavelength, 40 nm linewidth, 0.3 dB loss) was used in place of the previous filters for improved background rejection. Note that in space applications, only three sources of background light will need to be considered, which are the sun, the moon and earth, the positions of which are known and can be considered in mission planning. The receiver field of view will then be a trade-off between pointing accuracy requirements and exclusion of background sources. Both transmitter and receiver were mounted on camera tripods with additional pitch and yaw translation stages to aid in alignment. Figures 11(b) and (c) show the receiver and transmitter systems respectively. Figure 11(d) shows a photograph of the transmitter taken using a 300 mm lens from the receiver location, 750 m away. When the transmitter is aligned to point in the direction of the receiver, the transmitted light is visible by eye at this distance, despite the low emitted power of 463 μW.

Once the optical alignment had been optimized, BER measurements were taken for various data rates, transmitting over 10^5 bits in each case. The results are shown in Fig. 12. At 10 and 20 Mb/s error-free transmission was observed, reaching the error floor of 10^{-5}. For a data rate of 50 Mb/s, the FEC threshold was not reached, with a measured BER of 2.30×10^{-2}. At 100 Mb/s the BER was 4.02×10^{-1}.

Optics EXPRESS

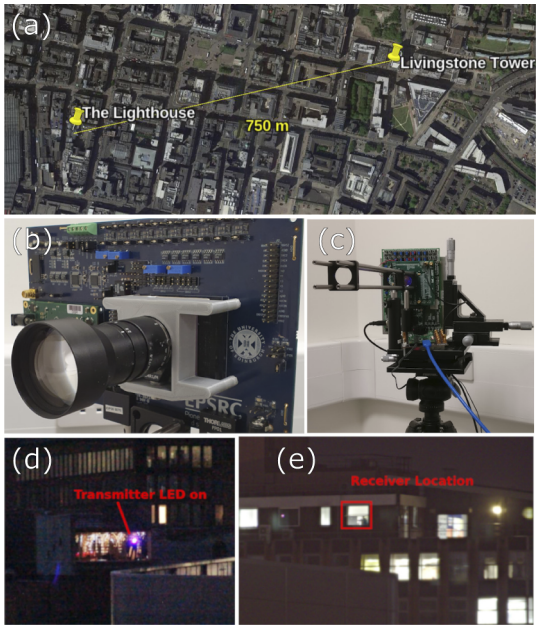

Fig. 11. (a) map of Glasgow city with the link indicated (© Google). Geographical coordinates: 55°51′38.16″ N, 4°15′0″ W, (b) receiver setup with camera optics for the 750 m link, (c) transmitter setup mounted on camera tripod, (d) photograph of aligned single micro-LED transmitter, taken from the receiver 750 m away, (e) photograph of the receiver location, taken from the transmitter.

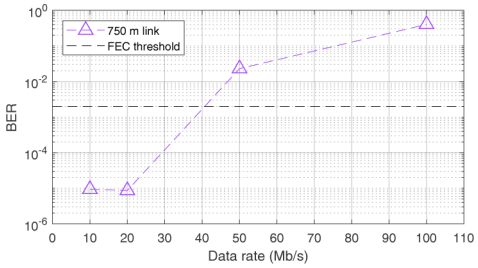

Fig. 12. BER performance at different data rates for a 750 m link between The Lighthouse and Livingston Tower in Glasgow.

Optics EXPRESS

For comparison between simulated conditions and the experimental implementation, the simulations were performed with adjusted parameters, specific to the demonstrator system. The measured output optical power of the micro-LED for each data rate is shown in Table 7, and the receiver lens diameter was 3.57 cm. The transmission losses through the receiver lens at 450 nm were also accounted for. The resulting range and coverages for different data rates are shown in Fig. 13, and the point-to-point ranges are summarized in Table 7.

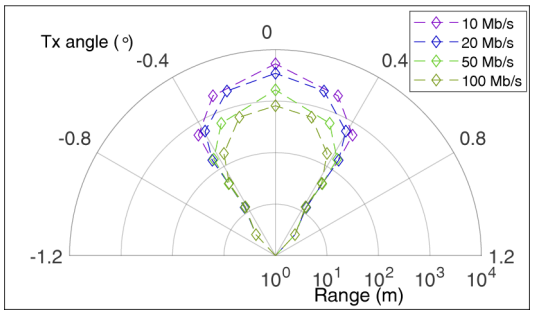

Fig. 13. Simulation of range performance for the implemented experimental setup , indicating that a 20 Mb/s link with a BER of 2×10^{-3} should be achievable for a 750 m link.

Table 7. Expected point-to-point ranges for the experimentally measured micro-LED emitted power and power collected through the lens (Tx power) at each data rate.

Data rate (Mb/s)	LED emitted power (μW)	Tx power (μW)	Point-to-point range (m)
10	806	542	5,321
20	689	463	3,483
50	390	262	1,656
100	188	126	815

Based on the simulation, it would be expected that all data rates up to 100 Mb/s should be achievable at the 750 m demonstration range. However, some variation from the simulation is to be expected, as there are additional channel losses in this ground-based demonstration which are difficult to account for. These include: transmission losses through glass windows, atmospheric absorption and scattering effects, and sub-optimal alignment on both a component and system level. All these factors will reduce the total power that reaches the receiver, and therefore reduce the achievable range significantly. In addition, despite night conditions, background light may increase the required incident power to achieve a BER of 2×10^{-3}. Nevertheless, the experimentally achieved data rate falls within the performance envelope defined by simulation. Due to the unknown channel losses it is not possible to determine the experimentally achieved directional gain accurately. However, by comparison of Figs. 2 and 12 and Table 7 we can estimate a lower boundary which is 42 dBi.

The ranges and data rates demonstrated experimentally are summarised in Table 8 for each transmitter lens. Note that due to experimental constraints some of these experiments had a BER below 2×10^{-3} and, therefore, a longer range is possible. The fact that these results experimentally verify several hundred meter ranges is very promising, and data rates in excess of 10 Mb/s are more than sufficient for the transmission of satellite command, health and navigation data, and potentially data payloads as well [18].

Optics EXPRESS

Table 8. Experimentally achieved ranges and data rates for the three transmitter optics.

Setup	Range (m)	Data rate (Mb/s)	BER
No lens	1.84	100	2×10^{-3}
C240	70	100	6×10^{-4}
ACL25416	750	20	$\leq 1 \times 10^{-5}$

4. Conclusion and future prospects

The expected deployment of clusters or constellations of small satellites inherently requires ISLs on strict SWaP budgets. Optical communication with LED transmitters is an attractive technology for this due to its simplicity, robustness, low SWaP and low cost nature. Here, we have experimentally demonstrated an optical communication link based on a single micro-LED and a SPAD receiver, achieving high data rates and sensitivities under a SWaP budget suitable for CubeSat systems. Data rates up to 100 Mb/s have been experimentally demonstrated with a sensitivity of −55.2 dBm, 13.42 dB from the SQL. This sensitivity is complemented by a directional gain of up to 52 dBi, which to our knowledge has not been achieved with a different technology under the same SWaP constraints. While the decoding was performed offline here, the digital nature of the system will enable full decoding using digital electronics in the future, with increased dynamic range.

In order to justify the application of this communication system to ISLs, ray-tracing simulations have been presented. Achievable ranges vary with many factors in the implementation, but a 100 Mb/s link can be maintained over a 5.74 km range with a simple optical system. Reducing target data rate to 10 kb/s permits 574 km ranges. Additionally, the divergent micro-LED emission can significantly relax the requirements on pointing accuracy for the satellite, where a 17 mrad accuracy will be sufficient for 140 km range, and 7 mrad for 570 km. Depending on the application scenario, it may be beneficial to operate the transmitter with no optics, as a low-range wide-angle broadcast system. A long distance link was experimentally verified, demonstrating error-free transmission at 20 Mb/s over a distance of 750 m. In this work, the link performance was carried out using a single LED within a micro-scle LED array. An additional benefit from using micro-LED sources in array format is that they may facilitate angular alignment of small satellites, based on multiple emission beams [43]. Such an alignment method would enable to achieve the required pointing accuracy without increasing the SWaP footprint.

This work paves the way for employing chip-scale optoelectronic emitters and receivers for low SWaP ISLs. We envisage that future research may extend to other chip-scale transmitter technologies. In particular, vertical cavity surface emitting lasers (VCSELs) are an interesting technology, because they can be fabricated in array format, have high modulation bandwidths, and offer narrow emission linewidth which is beneficial for background rejection. However, blue-emitting VCSELs have not yet reached the maturity needed for this application and near-infrared VCSELs are not well matched to the peak sensitivity of silicon SPADs. Their application to ISLs would be an interesting topic for future research.

Funding. Engineering and Physical Sciences Research Council (EP/M01326X/1, EP/S001751/1).

Acknowledgments. The authors would like to thank Jonathan McKendry and Daniel MacLure for assisting with the long distance experiment, and The Lighthouse for allowing access to the viewing platform.

Disclosures. The authors declare no conflicts of interest.

Data availability. Data underlying the results presented in this paper are available in Refs. [44], [45] and [46]. Video documentation of the long distance measurement (Visualization 1) is available at Ref. [42].

References

1. M. N. Sweeting, "Modern Small Satellites - Changing the Economics of Space," Proc. IEEE **106**(3), 343–361 (2018).

Optics EXPRESS

2. H. Kaushal and G. Kaddoum, "Optical Communication in Space: Challenges and Mitigation Techniques," IEEE Commun. Surv. Tutorials **19**(1), 57–96 (2017).
3. Z. Sodnik, B. Furch, and H. Lutz, "Optical inter-satellite communication," IEEE J. Sel. Top. Quantum Electron. **16**(5), 1051–1057 (2010).
4. M. A. Khalighi and M. Uysal, "Survey on free space optical communication: A communication theory perspective," IEEE Commun. Surv. Tutorials **16**(4), 2231–2258 (2014).
5. M. Gregory, F. Heine, H. Kämpfner, R. Meyer, R. Fields, and C. Lunde, "TESAT laser communication terminal performance results on 5.6Gbit coherent inter satellite and satellite to ground links," in *International Conference on Space Optics — ICSO 2010*, vol. 10565 E. Armandillo, B. Cugny, and N. Karafolas, eds., International Society for Optics and Photonics (SPIE, 2017), pp. 324–329.
6. F. Heine, H. Kämpfner, R. Lange, R. Czichy, R. Meyer, and M. Lutzer, "Optical inter-satellite communication operational," *Proceedings - IEEE Military Communications Conference MILCOM* pp. 1583–1587 (2010).
7. R. Radhakrishnan, W. W. Edmonson, F. Afghah, R. M. Rodriguez-Osorio, F. Pinto, and S. C. Burleigh, "Survey of Inter-Satellite Communication for Small Satellite Systems: Physical Layer to Network Layer View," IEEE Commun. Surv. Tutorials **18**(4), 2442–2473 (2016).
8. S. Janson, R. Welle, T. Rose, D. Rowen, B. Hardy, R. Dolphus, P. Doyle, A. Faler, D. Chien, A. Chin, G. Maul, C. Coffman, S. D. L. Lumondiere, I. Nicolette, and D. Hinkley, "The NASA Optical Communications and Sensor Demonstration Program : Initial Flight Results," *29th Annual AIAA/USU Conference on Small Satellities* pp. SSC16-III–03 (2015).
9. E. Clements, R. Aniceto, D. Barnes, D. Caplan, J. Clark, I. del Portillo, C. Haughwout, M. Khatsenko, R. Kingsbury, M. Lee, R. Morgan, J. Twichell, K. Riesing, H. Yoon, C. Ziegler, and K. Cahoy, "Nanosatellite optical downlink experiment: design, simulation, and prototyping," Opt. Eng. **55**(11), 111610 (2016).
10. R. Morgan and K. Cahoy, "Nanosatellite Lasercom System," *AIAA/USU Conference on Small Satellites* (2017).
11. R. Welle, A. Utter, T. Rose, J. Fuller, K. Gates, B. Oakes, and S. Janson, "A CubeSat-Based Optical Communication Network for Low Earth Orbit," *AIAA/USU Conference on Small Satellites* (2017).
12. S. Rajbhandari, J. J. D. Mckendry, J. Herrnsdorf, H. Chun, G. Faulkner, H. Haas, I. M. Watson, D. O. Brien, and M. D. Dawson, "A review of Gallium Nitride LEDs for multi-gigabit-per-second visible light data communications," Semicond. Sci. Technol. **32**(2), 023001 (2017).
13. H. Haas, L. Yin, Y. Wang, and C. Chen, "What is LiFi ?" J. Lightwave Technol. **34**(6), 1533–1544 (2016).
14. D. Chitnis, L. Zhang, H. Chun, S. Rajbhandari, G. Faulkner, D. O'Brien, and S. Collins, "A 200 Mb/s VLC demonstration with a SPAD based receiver," 2015 IEEE Summer Top. Meet. Series, SUM 2015 **3**, 226–227 (2015).
15. B. S. Robinson, D. O. Caplan, M. L. Stevens, R. J. Barron, E. A. Dauler, and S. A. Hamilton, "1.5-photons/bit Photon-Counting Optical Communications Using Geiger-Mode Avalanche Photodiodes," *LEOS Summer Topical Meetings* (2005).
16. B. Robinson, A. J. Kerman, E. A. Dauler, R. J. Barron, D. O. Caplan, M. L. Stevens, J. J. Carney, S. A. Hamilton, J. K. W. Yang, and K. K. Berggren, "781 Mbit/s photon-counting optical communications using a superconducting nanowire detector," Opt. Lett. **31**(4), 444–446 (2006).
17. L. Wood, W. Ivancic, and K. P. Dörpelkus, "Using light-emitting diodes for intersatellite links," *IEEE Aerospace Conference Proceedings* (2010).
18. D. N. Amanor, W. W. Edmonson, and F. Afghah, "Inter-Satellite Communication System based on Visible Light," IEEE Trans. Aerosp. Electron. Syst. **54**(6), 2888–2899 (2018).
19. J. J. D. McKendry, B. R. Rae, Z. Gong, K. R. Muir, B. Guilhabert, D. Massoubre, E. Gu, D. Renshaw, M. D. Dawson, and R. K. Henderson, "Individually addressable AlInGaN micro-LED arrays with CMOS control and subnanosecond output pulses," IEEE Photonics Technol. Lett. **21**(12), 811–813 (2009).
20. S. Zhang, S. Watson, J. J. D. McKendry, D. Massoubre, A. Cogman, E. Gu, R. K. Henderson, A. E. Kelly, and M. D. Dawson, "1.5 Gbit/s multi-channel visible light communications using CMOS-controlled GaN-based LEDs," J. Lightwave Technol. **31**(8), 1211–1216 (2013).
21. A. D. Griffiths, M. S. Islim, J. Herrnsdorf, J. J. D. McKendry, R. Henderson, H. Haas, and E. Gu, "CMOS-integrated GaN LED array for discrete power level stepping in visible light communications," Opt. Express **25**(8), A338–A345 (2017).
22. L. Zhang, D. Chitnis, H. Chun, S. Rajbhandari, G. Faulkner, D. C. O'Brien, and S. Collins, "A comparison of APD and SPAD based receivers for visible light communications," J. Lightwave Technol. **36**(12), 2435–2442 (2018).
23. O. Almer, D. Tsonev, N. A. Dutton, T. Al Abbas, S. Videv, S. Gnecchi, H. Haas, and R. K. Henderson, "A SPAD-based visible light communications receiver employing higher order modulation," *2015 IEEE Global Communications Conference, GLOBECOM 2015* pp. 0–5 (2015).
24. S. Gnecchi, N. A. Dutton, L. Parmesan, B. R. Rae, S. Pellegrini, S. J. McLeod, L. A. Grant, and R. K. Henderson, "Analysis of Photon Detection Efficiency and Dynamic Range in SPAD based Visible Light Receivers," J. Lightwave Technol. **34**(11), 2774–2781 (2016).
25. J. Kosman, O. Almer, T. A. Abbas, N. Dutton, S. Videv, K. Moore, H. Haas, and R. Henderson, "A 500Mb/s -46.1dBm CMOS SPAD receiver for laser diode visible-light communications," *IEEE International Solid-State Circuits Conference* pp. 15–17 (2019).

Optics EXPRESS

26. S. Gnecchi, N. A. Dutton, L. Parmesan, B. R. Rae, S. Pellegrini, S. J. McLeod, L. A. Grant, and R. K. Henderson, "Digital Silicon Photomultipliers With OR/XOR Pulse Combining Techniques," IEEE Trans. Electron. Devices **63**(3), 1105–1110 (2016).
27. B. Steindl, M. Hofbauer, K. Schneider-Hornstein, P. Brandl, and H. Zimmermann, "Single-Photon Avalanche Photodiode Based Fiber Optic Receiver for Up to 200 Mb/s," IEEE J. Sel. Top. Quantum Electron. **24**(2), 1–8 (2018).
28. H. Zimmermann, B. Steindl, M. Hofbauer, and R. Enne, "Integrated fiber optical receiver reducing the gap to the quantum limit," Sci. Rep. **7**(1), 2652 (2017).
29. W. Shieh and I. Djordjevic, *OFDM for optical communications* (Elsevier, London, 2010).
30. A. D. Griffiths, J. Herrnsdorf, M. J. Strain, and M. D. Dawson, "High sensitivity inter-satellite optical communications using leds and single photon receivers," in *The Eleventh International Conference on Advances in Satellite and Space Communications*, (2019).
31. ITU, Geneva, Switzerland, "Recommendation G.975.1: forward error correction for high bit-rate DWDM submarine systems," (2005).
32. Y. Kawamura and T. Tanaka, "Transmission of the LED light from the space to the ground," AIP Adv. **3**(10), 102110 (2013).
33. X. Sun, P. L. Jester, S. P. Palm, J. B. Abshire, J. D. Spinhirne, and M. A. Krainak, "In orbit performance of Si avalanche photodiode single photon counting modules in the Geoscience Laser Altimeter System on ICESat," in *Advanced Photon Counting Techniques*, vol. 6372 W. Becker, ed., International Society for Optics and Photonics (SPIE, 2006), pp. 183–190.
34. M. Yang, F. Xu, J.-G. Ren, J. Yin, Y. Li, Y. Cao, Q. Shen, H.-L. Yong, L. Zhang, S.-K. Liao, J.-W. Pan, and C.-Z. Peng, "Spaceborne, low-noise, single-photon detection for satellite-based quantum communications," Opt. Express **27**(25), 36114–36128 (2019).
35. Y. C. Tan, R. Chandrasekara, C. Cheng, and A. Ling, "Silicon avalanche photodiode operation and lifetime analysis for small satellites," Opt. Express **21**(14), 16946–16954 (2013).
36. E. Anisimova, B. L. Higgins, J.-P. Bourgoin, M. Cranmer, E. Choi, D. Hudson, L. P. Piche, A. Scott, V. Makarov, and T. Jennewein, "Mitigating radiation damage of single photon detectors for space applications," EPJ Quantum Technol. **4**(1), 10 (2017).
37. D. Milovancev, J. Weidenauer, B. Steindl, M. Hofbauer, R. Enne, and H. Zimmermann, "Influence of On-Off Keying Duty Cycle on BER in Wireless Optical Communication Up to 75 Mbit/s Using an SPAD and a RC LED," *Proceedings - 2018 International Conference on Broadband Communications for Next Generation Networks and Multimedia Applications, CoBCom 2018* pp. 1–5 (2018).
38. A. D. Griffiths, J. Herrnsdorf, O. Almer, R. K. Henderson, M. J. Strain, and M. D. Dawson, "High-sensitivity free space optical communications using low size, weight and power hardware," arXiv:1902.00495 (2019).
39. J. J. D. McKendry, D. Massoubre, S. Zhang, B. R. Rae, R. P. Green, E. Gu, R. K. Henderson, A. E. Kelly, and M. D. Dawson, "Visible-Light Communications Using a CMOS-Controlled Micro-Light- Emitting-Diode Array," J. Lightwave Technol. **30**(1), 61–67 (2012).
40. J. A. Richardson, L. A. Grant, and R. K. Henderson, "Low dark count single-photon avalanche diode structure compatible with standard nanometer scale CMOS technology," IEEE Photonics Technol. Lett. **21**(14), 1020–1022 (2009).
41. T. A. Abbas, N. A. W. Dutton, O. Almer, N. Finlayson, F. M. D. Rocca, and R. Henderson, "A CMOS SPAD Sensor with a Multi-Event Folded Flash Time-to-Digital Converter for Ultra-fast Optical Transient Capture," IEEE Sensors J. **18**(8), 3163–3173 (2018).
42. J. Herrnsdorf, A. D. Griffiths, J. J. D. McKendry, D. Maclure, R. Henderson, M. D. Dawson, and M. J. Strain, "Wireless data transmission at 20 mb/s over 750 m distance using a single microscopic blue led and a single photon avalanche diode detector chip," https://doi.org/10.15129/3da7087a-91a3-40be-9a83-7e412156db59 (2020).
43. J. Herrnsdorf, A. D. Griffiths, C. Lowe, M. Macdonald, M. J. Strain, and M. D. Dawson, "Towards using LED Arrays for Relative Alignment of Cube Satellite Clusters," *2019 IEEE Photonics Conference, IPC 2019 - Proceedings* pp. 1–2 (2019).
44. A. D. Griffiths, "Rz-ook data for optical communications with a micro-led and spad array," http://dx.doi.org/10.15129/fe315481-2a4a-4b84-a8ea-b239ddf27074 (2019).
45. A. D. Griffiths, "Zemax simulation data for led/spad communication ranges and coverages," http://dx.doi.org/10.15129/cb3af47d-3d40-49d6-8cf6-52c13fcf1769 (2019).
46. A. D. Griffiths and J. Herrnsdorf, "Communication data for a 750 m optical link using a micro-led and single photon avalanche diode array," https://doi.org/10.15129/6e0c2a04-35bc-4d45-b623-c72db9d94f2d (2021).